TECHNICAL RESEARCH REPORT

Multiobjective Optimization of a Leg Mechanism with Various Spring Configurations for Force Reduction

by W-B. Shieh, L-W. Tsai,
S. Azarm, A.L. Tits

T.R. 96-52

ISR
INSTITUTE FOR SYSTEMS RESEARCH

Sponsored by
the National Science Foundation
Engineering Research Center Program,
the University of Maryland,
Harvard University,
and Industry

MULTIOBJECTIVE OPTIMIZATION OF A LEG MECHANISM WITH VARIOUS SPRING CONFIGURATIONS FOR FORCE REDUCTION

W.-B. Shieh[1] L.-W. Tsai[2] S. Azarm[3] A.L. Tits[4]

Mechanical Engineering Department[1,2,3]
Institute for Systems Research[2,4]
Electrical Engineering Department[4]

University of Maryland
College Park, Maryland 20742

ABSTRACT In this paper, the design of a two degree-of-freedom leg mechanism is accomplished by a two-stage optimization process. In the first stage, leg dimensions are optimized with respect to three design objectives: minimize (i) leg size, (ii) vertical actuating force, and (iii) peak crank torque for an entire walking cycle. Following the optimization of leg dimensions, in the second stage, spring elements with various placement configurations are considered for further reduction of the actuating force and crank torque. Several tradeoff solutions are obtained and a comparison between various spring configurations is made. It is shown that the inclusion of spring elements can significantly reduce the actuating force and crank torque.

1 INTRODUCTION

A wide variety of leg mechanisms for walking machines have been proposed in the literature over the past few decades (Todd, 1985). For example, the Adaptive Suspension Vehicle (Waldron et al., 1984; Pugh et al., 1990) and TITAN III (Hirose, 1984) used pantograph-type mechanism to provide two degrees of freedom (DOFs) for each leg. A third DOF was obtained by rotating the pantograph as a whole about an axis fixed on the frame of the vehicle. This pantograph-type leg mechanism is flexible and efficient in terms of energy loss. However, all three DOFs must be actively controlled even for walking on a flat terrain, resulting in machines with complex control architecture and slow speed. On the other hand, Funabashi(1985a; 1985b) used a one-DOF multiple-bar linkage as a leg mechanism in his biped machine to generate an ovoid foot-path with a continuously rotating crank (motor). Although this type of mechanism

can achieve fast locomotion with minimal control, it lacks the flexibility required for avoiding obstacles and climbing stairs.

In a recent paper, a compound two DOF leg mechanism proposed by Williams et al.(1991) was studied (Shieh et al., 1994). The compound mechanism consists of a four-bar linkage and a pantograph. It generates an ovoid foot-path with a continuously rotating crank and therefore it requires minimal control and consumes very little propelling energy when walking on a flat terrain. It also provides a second DOF for obstacle avoidance and a third DOF for turning capability. It was shown that the design of such a complex mechanism can be accomplished by a multiobjective optimization procedure including many geometric and structural constraints, without the need of a prescribed coupler-point path. That study was preliminary, in that the model emphasized the driving torque of the forward-and-backward motion, while the vertical actuating force of the up-and-down movement was not included as a design objective. Since the actuator size of a leg mechanism is crucial to the performance of a walking machine, a comprehensive design methodlogy should take into account both actuating force and torque. Additionally, such a methodology should also accomodate the placement of a set of light weight passive elements, such as springs, on the leg mechansim in order to further reduce the actuating force and torque. Spring elements have been used in leg mechanisms both to store kinetic energy (Alexander, 1990; Dhandapani and Ogot, 1994) and to reduce actuating forces (Shin and Streit, 1993). In Shin and Streit(1993), a two-DOF equilibrator (the leg) and an extra mechanism which switches alternatively between the propelling and returning phases in a walking cycle was implemented. While such an equilibrator allows a significant reduction in actuating forces, the extra mechanism used in the equilibrator leg requires a complicated control algorithm even for flat terrain walking.

In this paper, we present a two-stage optimization procedure for the design of the compound mechanism shown in Fig. 1 that addresses the issues just outlined. In the first-stage, leg dimensions are optimized by simultaneously minimizing: (i) the leg size, (ii) the vertical actuating force, and (iii) the peak crank torque, subject to several geometric constraints. In the second-stage optimization, we reduce the actuating force and torque by directly placing spring elements on the mechanism. Further reduction of the actuating force and torque for the entire walking cycle is achieved by optimizing the size and the attachment points of a set of tension springs. This is different from the approach suggested by Matthew and Tesar(1977a; 1977b) who develped an analytic solution to meet external force and torque requirements at a finite number of points.

The balance of this paper is organized as follows. In Section 2, a description of the leg mechanism is

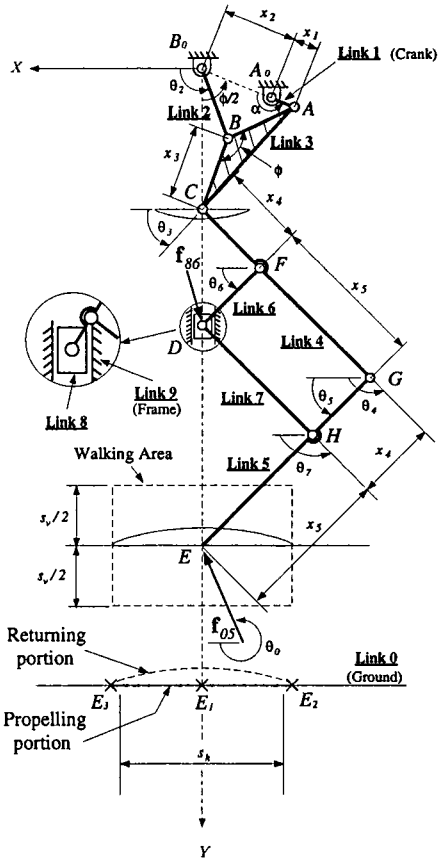

FIGURE 1: The compound leg mechanism

reviewed. In Section 3, we describe the first-stage optimization of the mechanism, including the formulation of design objectives and constraint functions, and the optimization results. In Section 4, three different configurations for the placement of springs are presented and the second-stage optimization results are discussed. Finally, concluding remarks are given in Section 5.

2 MECHANISM DESCRIPTION

A planar two-DOF mechanism (Williams et al., 1991) composed of a four-bar linkage A_0AB_0B and a pantograph $CDEFGH$ is shown in Fig. 1. One end of the pantograph is driven by the four-bar coupler point C, while the other end D is driven by a linear actuator. Rotation of the crank provides a back-and-forth motion, while linear motion of point D provides an up-and-down motion of the foot point E. A third-DOF motion (not shown in the figure) providing a turning capability is achieved by allowing the planar mechanism to rotate about a vertical axis fixed on the frame of the walking machine. In this study, we concentrate only on the planar portion of the leg mechanism. For convenience, an X-Y reference

coordinate system with its Y-axis pointing downward in the direction of $\overrightarrow{B_0D}$ and with its origin located at joint B_0 is defined in Fig. 1.

The first DOF, rotation of crank A_0A, is used to generate an ovoid path for normal walking on a flat terrain. Such a path enables the walking machine to step over small obstacles (rocks or trenches) without raising its body too much or applying the second DOF motion. In our design, the four-bar linkage is selected such that $\overline{AB} = \overline{BC} = \overline{B_0B}$ and the angle ($\angle DB_0A_0$) between the symmetric axis $\overrightarrow{B_0D}$ and the four-bar linkage baseline $\overrightarrow{B_0A_0}$ is equal to $\phi/2$, where $\phi = \angle ABC$. It is well known (Hartenberg and Denavit, 1964) that for this type of four-bar linkage the coupler-point curve traced by the point C is symmetric about the axis $\overrightarrow{B_0D}$. The pantograph, which is connected to the four-bar linkage at point C, reproduces and amplifies the coupler-point curve by a factor of $(-x_5/x_4)$ at the foot-point E. The negative sign refers to the inverted shape of the curve generated by point E as compared to that generated by point C. For simplicity, the amplification factor (x_5/x_4) is denoted as n hereafter. The joint D is guided along the symmetry axis to provide a specified vertical stride s_v.

The curve traced by the foot-point path consists of two portions: a propelling portion and a returning portion. The propelling portion of the foot-point path is that portion of the curve where the foot makes contact with the ground (line $E_3E_1E_2$). Points E_2 and E_3 are the two extreme positions of the foot path traced by E where $dX_E/d\alpha = 0$. The distance between these two positions E_2E_3, which are symmetric about the Y-axis, is referred to as the horizontal stride. Note that the horizontal stride must be no smaller than the desired stride s_h, as shown in Fig. 1. Due to symmetry, the crank angles at the two positions, E_2 and E_3, separating the propelling and returning portions are also symmetric about $\alpha = 0$ (Hartenberg and Denavit, 1964).

3 FIRST-STAGE OPTIMIZATION: LEG DIMENSIONS

The problem of determining leg dimensions, spring size, and spring placement for the mechanism just described can be formulated as a constrained multiobjective optimization problem. We decompose the optimization process into two stages. In the first-stage optimization, the design variables (see Fig. 1), dimensions x_1 through x_5 and the coupler angle ϕ, are determined. Then springs are added in the second-stage optimization, with their size and placement optimized, to further reduce the driving torque and actuating force. All of these subject to various mechanism constraints. Such complexity in the number of design variables, constraints and objectives calls for numerical optimization. We used Consol-Optcad (Fan et al., 1990), an interactive optimization-based design package, to achieve these goals.

3.1 Objective Functions

Three design objectives are simultaneously considered in the optimization model: minimize (i) the leg size, (ii) the vertical actuating force at joint D, and (iii) the peak crank torque on a flat walking terrain.

Objective 1: minimizing the leg size.

Since the configuration of the leg mechanism changes as a function of the crank angle and the joint D displacement, the problem of computing the leg size will become unnecessarily complex if it is to be calculated at all configurations. For simplicity, the leg size is only calculated at the configuration shown in Fig. 1, where point E is at the middle of the propelling portion and joint D at the middle of its vertical operating range. At this particular configuration, the crank angle α is taken to be π. [1] Since the pantograph as shown in Fig. 1 has its two links $\overline{CG} = \overline{GE}$ and the transmission angle of the pantograph at the normal configuration is selected to be $\pi/2$, the leg height $\overline{B_0E}$ can be derived as,

$$\overline{B_0E} = Y_C|_{\alpha=\pi} + \sqrt{2}(x_4 + x_5) \tag{1}$$

where Y_C can be found in Appendix A. The width w of leg mechanism is defined as the maximum X coordinate of joint A or G, i.e.

$$\begin{aligned} w &= \max(X_A, X_G) \\ &= \max[(x_1 + x_2)\sin(\phi/2), \sqrt{2}(x_4 + x_5)/2]. \end{aligned} \tag{2}$$

Normalizing the leg size with respect to a prespecified walking area $(s_v s_h)$ yields

$$\mathtt{O1} := \frac{[Y_C|_{\alpha=\pi} + \sqrt{2}(x_4 + x_5)]\max(X_A, X_G)}{s_v s_h}. \tag{3}$$

Therefore, the first design objective is: $\min_{\mathbf{x}} \{\mathtt{O1}\}$.

Objective 2: minimizing the vertical actuating force. Since the vertical actuating force f_{86Y} at joint D is related to the ground reaction force f_{05Y} by a factor of $-(1+n)$,

$$\mathtt{O2} := f_{86Y} = -(1+n)f_{05Y}. \tag{4}$$

Hence our second design objective is : $\min_{\mathbf{x}} \{\mathtt{O2}\}$.

Objective 3: minimizing the peak crank torque. Assuming that the transmission loss between the input crank and the output foot point is negligible, the input and output powers are equal:

$$T\frac{d\alpha}{dt} = f_{50X}\frac{dX_E}{dt} + f_{50Y}\frac{dY_E}{dt}. \tag{5}$$

[1] α could be taken to be zero as well.

Rearranging Eq. (5) results in a functional objective

$$\texttt{F01} := T = -f_{05X}\frac{dX_E}{d\alpha} - f_{05Y}\frac{dY_E}{d\alpha} \qquad \forall\, \alpha \in R_p. \tag{6}$$

Note that $f_{50X} = -f_{05X}$ and $f_{50Y} = -f_{05Y}$. Also note that torque T remains unchanged as joint D moves up and down. Thus our third design objective (which is in a functional form, i.e., a function of design variables and a free variable α, $\alpha \in R_p$) is: $\min_{\mathbf{x}} \{\texttt{F01}\}$.

3.2 Constraint Functions

The mechanism constraint functions refer to the constraints imposed on the geometry of the linkage and foot-point path. All the constraints on length or distance are normalized.

Stride length. The horizontal stride is defined as the distance from E_2 to E_3 (see Fig. 1). The corresponding crank angles at E_2 and E_3 are denoted as $\alpha = \alpha_x$ and $\alpha = -\alpha_x$, respectively. The angle α_x is obtained numerically by setting $dX_E/d\alpha = 0$. Due to symmetry, $\overline{E_1E_3} = \overline{E_1E_2}$. Hence, the constraint on the stride length is

$$\texttt{C1} := \frac{2X_E|_{\alpha=\alpha_x}}{s_h} \geq \texttt{H}_{\texttt{C1}}. \tag{7}$$

Normally the threshold $\texttt{H}_{\texttt{C1}}$ is 1 since the foot-path stride should be no less than a prespecified stride length s_h.

Foot-path height. The height of the foot path is the difference between the Y coordinate of the foot-point E at $\alpha = 0$ and $\alpha = \pi$,

$$\texttt{C2} := \frac{Y_E|_{\alpha=\pi} - Y_E|_{\alpha=0}}{s_h} \geq \texttt{H}_{\texttt{C2}} \tag{8}$$

where the value of $\texttt{H}_{\texttt{C2}}$ is positive.

Four-bar transmission angle. Since $\overline{AB} = \overline{B_0B} = x_3$, the minimum and maximum transmission angles, C3 and C4, of the four-bar linkage, can be written as

$$\texttt{C3} := 2\sin^{-1}\left(\frac{x_2 - x_1}{2x_3}\right) \geq \texttt{H}_{\texttt{C3}} \tag{9}$$

$$\texttt{C4} := 2\sin^{-1}\left(\frac{x_2 + x_1}{2x_3}\right) \leq \texttt{H}_{\texttt{C4}}. \tag{10}$$

To achieve efficient force transmission in the four-bar linkage, the transmission angle should not deviate too much from $\pi/2$. In this paper, $\texttt{H}_{\texttt{C3}}$ and $\texttt{H}_{\texttt{C4}}$ are chosen such that $(\pi/2 - \texttt{H}_{\texttt{C3}}) = (\texttt{H}_{\texttt{C4}} - \pi/2)$. Note that under this constraint the Grashof criteria for the four-bar linkage are automatically satisfied.

Pantograph transmission angle. The pantograph becomes singular when all its links are aligned, i.e., ΔCGE collapses to a straight line. The singularity of a pantograph is avoided as long as ΔCGE remains a bona fide triangle throughout a full crank cycle. Again, to achieve this, the transmission angle $\angle CGE$ should not deviate too much from $\pi/2$. Hence, the minimum and maximum transmission angles of the pantograph, C5 and C6, are

$$\mathtt{C5} := \cos^{-1}\left[\frac{2(x_4+x_5)^2 - l_{min}^2}{2(x_4+x_5)^2}\right] \geq \mathtt{H_{C5}} \tag{11}$$

$$\mathtt{C6} := \cos^{-1}\left[\frac{2(x_4+x_5)^2 - l_{max}^2}{2(x_4+x_5)^2}\right] \leq \mathtt{H_{C6}} \tag{12}$$

where l_{min} and l_{max} are the minimum and maximum distances of $\overline{CE}$, respectively, and can be easily obtained from Fig. 1. The thresholds $\mathtt{H_{C5}}$ and $\mathtt{H_{C6}}$ are chosen such that $(\pi/2 - \mathtt{H_{C5}}) = (\mathtt{H_{C6}} - \pi/2)$.

Links 4 and 5 orientation angles. In order to prevent link 4 from interfering with the four-bar linkage or link 5 from bumping into the ground, the orientations of these two links must be constrained. Since the link lengths $\overline{CG} = \overline{GE}$, the minimum and maximum angles of θ_5 are equal to those of $\pi - \theta_4$. Therefore one constraint would be enough,

$$\mathtt{FC1} := \theta_5 \geq \mathtt{H_{FC1}}, \qquad \forall\, \alpha \in R_p. \tag{13}$$

The quantity θ_5 can be obtained by subtracting $\angle GEC$ from the orientation of $\overrightarrow{CD}$,

$$\theta_5 = \cos^{-1}\left(\frac{X_C}{U}\right) - \cos^{-1}\left(\frac{U}{2x_4}\right) \tag{14}$$

where $U = [{X_C}^2 + {Y_C}^2 + {Y_D}^2 - 2Y_C Y_D]^{1/2}$.

Second derivatives of Y_E. Since the propelling portion of the foot path should be always below the non-propelling portion within the entire stride length, it is desirable to have the foot path concave upward ($-Y$ direction) for the entire propelling portion, i.e.

$$\mathtt{FC2} := \frac{d^2 Y_E}{d\alpha^2} \leq \mathtt{H_{FC2}}, \quad \text{for } \overline{E_2 E_3} \tag{15}$$

3.3 First-Stage Optimization Results: Leg Dimensions

The leg dimensions optimization was carried out based on the following specifications: (i) foot reaction force f_{05X} = 0 N, and f_{05Y} = -890 N (200 lb); (ii) horizontal (s_h) and vertical (s_v) stride lengths of 0.3 m (12 in) and 0.2 m (8 in), respectively; and (iii) walking on a flat terrain. In addition, the parameters of

	Initial Design	Optimized Designs						
		1	2	3	4	5	6	7
f_{86Y_u} [a]	N/A	2.75	3.00	3.25	3.50	3.75	4.00	4.25
f_{86Y_o}	2.67	2.38	2.55	2.75	3.00	3.25	3.56	3.85
x_1 (cm)	3.0	5.0	4.5	4.1	3.7	3.4	3.1	2.9
x_2 (cm)	14.0	21.3	19.4	17.8	16.4	15.6	15.4	14.5
x_3 (cm)	12.0	19.3	17.3	15.6	14.3	13.0	12.5	11.8
x_4 (cm)	15.0	13.8	12.4	11.2	10.1	9.1	8.3	7.7
x_5 (cm)	30.0	23.0	23.1	23.4	23.7	24.1	24.8	25.5
ϕ (rad)	3.00	2.20	2.17	2.14	2.09	2.05	2.00	2.00
$\mu_{\max}$ [b]	54.6	50.0	50.8	52.1	54.1	55.9	58.6	58.4
$\mu_{\min}$	94.9	85.6	87.3	89.3	91.6	93.6	95.5	94.9

[a] f_{86Y_u} and f_{86Y_o} are the upper bound and optimized values of the actuating force f_{86Y} (kN), respectively.
[b] $\mu_{\min}$ and $\mu_{\max}$ are the minimum and maximum of the transmission anlges (in degrees) of the four-bar linkage.

TABLE 1: Initial and Optimized Design variables

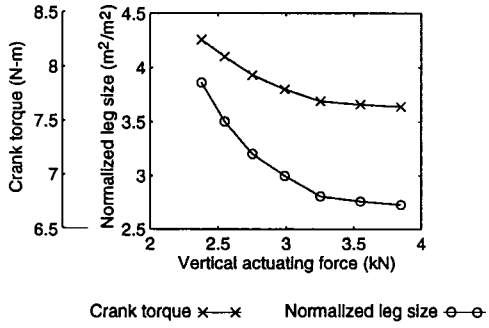

FIGURE 2: Leg size vs. f_{86Y} and crank torque vs. f_{86Y} for seven optimized solutions

constraints are chosen as follows: $H_{C1} = 1$; $H_{C2} = 0.08$; $H_{C3} = H_{C5} = 0.873$ radian (50 degrees); $H_{C4} = H_{C6} = 2.268$ radians (130 degrees); $H_{FC1} = 0.436$ radian (25 degrees); and $H_{FC2} = 0$.

Our main goal here is to investigate how the vertical actuating force affects the leg design in terms of the crank torque and leg size. As we gradually relaxed the limitations on the vertical actuating force at joint D, from 2.75 (kN) to 4.25 (kN) at an equal increment of 0.25 (kN), seven optimized leg designs, labeled 1 to 7, were obtained. The initial and seven optimized leg dimensions and their extreme transmission angles are shown in Table 1.

Fig. 2 shows the tradeoffs between the three design objectives. As the vertical actuating force increases from 2.38 kN to 3.85 kN, the normalized leg size decreases from 3.86 to 2.72. Similar trend can be observed for the crank torque curve in Fig. 2. However, as shown in Fig. 2, the impact of actuating force on leg size is much larger than that on the crank torque.

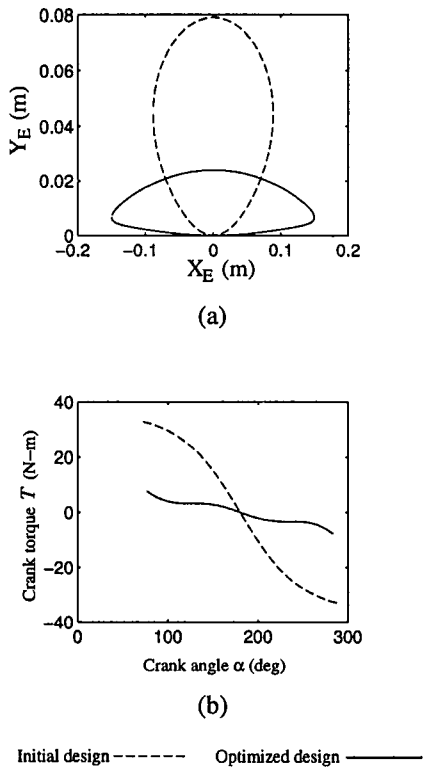

FIGURE 3: (a) Foot path; (b) Torque curve for an initial and optimized designs

Fig. 3(a) shows both the initial and optimized foot paths for the optimized design number 3 listed in Table 1. We note that the propelling portion (the lower portion) of the foot path becomes much flatter after optimization. Fig. 3(b) shows the crank torque variation during the propelling portion which has been substantially reduced after optimization.

4 SECOND-STAGE OPTIMIZATION: SPRING SIZE AND PLACEMENT

Since a large actuator will make the walking machine heavy and this in turn results in high reaction load at the foot point, it is desired to further reduce the already optimized torque and force obtained from the first-stage optimization. For this reason, light weight passive elements such as springs are considered. Among a variety of springs, tension spring is selected for its ease of attachment. Since there is no general guideline for mounting springs to the mechanism, the spring placement configuration should take advantage of some of the features of the mechanism. For our leg mechanism, symmetry is a significant feature. Thus, all of the springs are arranged in such a way that the actuator force and crank torque are reduced in a symmetric manner. In the following sections, three possible spring configurations as shown in Fig. 4 are presented for the reduction of the actuating force and torque.

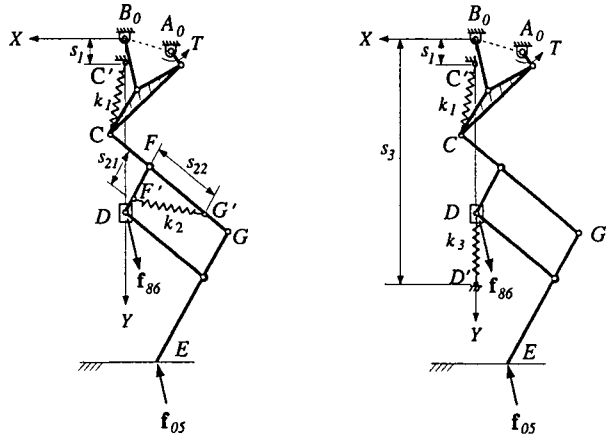

(a) Configuration I (b) ConfigurationII

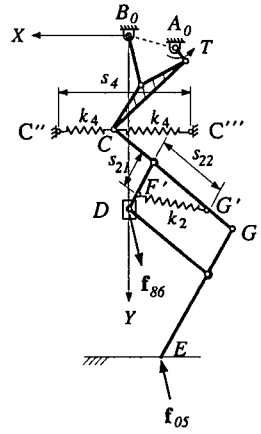

(c) Configuration III

FIGURE 4: Three proposed spring configurations

4.1 First Configuration

Fig. 4(a) shows two springs attached on the leg mechanism. Spring k_1 (k_1 is the spring constant) is connected at points C and C'. Point C' lies on the axis of symmetry B_0D and point C is the coupler point of the four-bar. Spring k_2 is attached onto the pantograph at G' and F', where point G' lies on link FG and point F' lies on link DF. As a result (see below), the crank torque is reduced by both springs, while the vertical actuating force at point D is reduced by spring k_2 alone.

Without the springs, when the mechanism is subject to a force $\mathbf{f}_{05}$, the pantograph will be under compression, i.e., points C and E tend to approach each other, while the coupler point C of the four-bar linkage tends to move away from its base point B_0. After the springs are attached on the mechanism,

spring k_1 will pull the coupler point C toward the base point B_0 and spring k_2 will extend the pantograph. Because of this, force acting on the coupler point C is affected by both springs, resulting in a reduced crank torque. As to the pantograph, a reduced actuating force at point D is obtained due to the fact that the compressive force from the ground is partially balanced by the tension force from spring k_2.

Applying the principle of virtual work (see details in Appendix B), we obtain the crank torque as

$$T = [nf_{05X} + (k_1\delta_1 - k_2\delta_2)X_C]\frac{dX_C}{d\alpha} + [nf_{05Y} + k_1\delta_1(Y_C - s_1) + k_2\delta_2(Y_D - Y_C)]\frac{dY_C}{d\alpha} \tag{16}$$

where $n = x_5/x_4$, $\delta_1 = (1 - l_{01}/l_1)$, and $\delta_2 = (s_{21}s_{22}/{x_4}^2)(1 - l_{02}/l_2)$. The coefficients of the $dX_C/d\alpha$ and $dY_C/d\alpha$ in Eq. (16) are respectively the X- and Y- forces at joint C. Note that in Eq. (16), f_{05Y} is always negative, while $k_1\delta_1(Y_C - s_1)$ and $k_2\delta_2(Y_D - Y_C)$ are always positive. Therefore, the crank torque can be substantially reduced as long as the term $(k_1\delta_1 - k_2\delta_2)$ is kept at a small value. The vertical actuating force at point D is

$$f_{86Y} = -(1 + n)f_{05Y} - k_2\delta_2(Y_D - Y_C). \tag{17}$$

Note that the right hand side of Eq. (17) is the difference of two positive quantities (since f_{05Y} is negative).

It can be seen from Eq. (16) that the resultant crank torque is affected by both springs. This implies that there are restrictions in the selection of springs, because of their coupling effect on crank torque. Note that in this configuration, an additional reaction force in the X- direction at point D is introduced by spring k_2, which will increase the frictional force of the slider at point D.

4.2 Second Configuration

Fig. 4(b) shows an alternative arrangement of the springs. Spring k_1 is attached at points C and C' identical to that shown for the first configuration, while spring k_3 is connected at points D and D', where point D' lies on the axis of symmetry B_0D. The crank torque T for this spring configuration, via a formulation similar to that described in Appendix B, is given by

$$T = (nf_{05X} + k_1\delta_1 X_C)\frac{dX_C}{d\alpha} + [nf_{05Y} + k_1\delta_1(Y_C - s_1)]\frac{dY_C}{d\alpha} \tag{18}$$

and the actuating force f_{86Y} is found to be

$$f_{86Y} = -(1 + n)f_{05Y} - k_3[(s_3 - Y_D) - l_{03}]. \tag{19}$$

From Eqs. (18) and (19), it is clear that the crank torque T depends only on spring k_1 and the actuating force f_{86Y} is solely related to spring k_3. Unlike the first configuration, there is no coupling effect between

these two springs. Moreover, k_3 spring will not generate additional side force at point D. However, one potential problem with this design is that the attachment point D' may come too close to the ground.

4.3 Third Configuration

The third spring configuration, as shown in Fig. 4(c), consists of three springs. Spring k_2 is attached to the pantograph at F' and G' identical to that of the first configuration. One end of two springs k_4 are attached at point C, while the other ends are attached at C'' and C''', respectively. Both C'' and C''', which are symmetric about the Y-axis, are located on a horizontal line passing half way between the two extreme Y coordinates of the coupler curve. Since the coupler point C does not change much in its Y coordinate (compared to the change in the X coordinate), the force generated by springs k_4 are mainly in the X-direction. Neglecting the Y-direction force generated by springs k_4, the crank torque T is obtained as

$$T = [nf_{05X} + (k_2\delta_2 - 2k_4)X_C]\frac{dX_C}{d\alpha} + [nf_{05Y} + k_2\delta_2(Y_C - s_1)]\frac{dY_C}{d\alpha} \tag{20}$$

and f_{86Y} is given by Eq. (17).

Note that, in this design, points C'' and C''' must be separated far enough for the springs to remain in tension at all times. This may pose a problem in a situation when the available space is limited. Similar to the second configuration, springs k_2 and k_4 are not coupled. Again, spring k_2 generates an additional frictional force on the slider point D.

4.4 Design Variables, Objectives, and Constraints

For the sizing and placement of the springs, an optimization-based model is established. The model is comparably simpler than that for the leg mechanism dimensions and again the software Consol-Optcad (Fan et al., 1990) is used.

The design variables for the three spring configurations include the distances s_1, s_{21}, s_{22}, s_3, and s_4, the spring constants k_1 through k_4, and their unstretched (or free) lengths l_{01} through l_{04}. All of the design variables are assumed to be positive, except s_1 which is allowed to be negative. Here, quantities s_1 and s_3 are measured from point B_0 along the Y-axis direction, while s_{21} and s_{22} are measured from point F along $\overrightarrow{FD}$ and $\overrightarrow{FG}$, respectively, and the quantity s_4 is defined as $\overline{C''C'''}$.

The design objectives of the second-stage optimization are the crank torque T and the actuating force f_{86Y}, as described in the previous sections. The constraints can be divided into two groups: constraints on

the extension ratios of the springs, and constraints on the location of the spring attachment points. For each spring, two constraints on the extension ratio are imposed. For example, spring k_1 has the following two constraints:

$$\mathtt{SC1} := \frac{\min(l_1)}{l_{01}} \geq \mathtt{H_{SC1}} \tag{21}$$

$$\mathtt{SC2} := \frac{\max(l_1)}{l_{01}} \leq \mathtt{H_{SC2}}. \tag{22}$$

The quantity $\mathtt{H_{SC1}}$, normally set to one, is the minimum extension ratio. The quantity $\mathtt{H_{SC2}}$, depending on the spring characteristics, is the maximum extension ratio. The stretched lengths l_1 and l_2 and their extreme values can be found in Appendix B, while $\min(l_3) = s_3 - \{Y_{D1} + sv/[2(1+n)]\}$, $\max(l_3) = s_3 - \{Y_{D1} - sv/[2(1+n)]\}$, $\min(l_4) = s_4/2 - X_E|_{\alpha=\alpha_x}$ and $\max(l_4) = s_4/2 + X_E|_{\alpha=\alpha_x}$ can be easily obtained from Fig. 4. Here $Y_{D1} = Y_C|_{\alpha=\pi} + \sqrt{2}x_4$ where Y_{D1} is the Y coordinate of slider D when it is held at its middle position, and $sv/[2(1+n)]$ is one-half of the vertical stride of slider D.

As to the constraints on the locations of the spring attachment points, agian we take spring k_1 as an example:

$$\mathtt{SC3} := s_1 \geq \mathtt{H_{SC3}} \tag{23}$$

$$\mathtt{SC4} := s_1 \leq \mathtt{H_{SC4}} \tag{24}$$

where $\mathtt{H_{SC3}}$ and $\mathtt{H_{SC4}}$ are the minimum and maximum values for s_1, respectively. Note that, for spring k_2, the maxima of s_{21} and s_{22} are desired to be smaller than x_4 and x_5, respectively. Therefore, a second-stage optimization model can be easily developed for each spring configuration using the objective and constraint functions described in this section.

4.5 Second-Stage Optimization Results: Spring Size and and Placement

The second-stage optimization results are obtained based on the following assumptions: (i) the maximum spring extension ratio for all springs is 30%; (ii) the spring constants are not to exceed 50 kN/m; (iii) joint D is held at the middle position while the crank torque and actuating force are computed for a full crank cycle; and (iv) leg dimensions obtained for design number 3 of Table 1 is used for all three spring configurations.

The spring constants and their unstretched lengths for the three optimized configurations are tabulated in Table 2, while the spring locations are listed in Table 3. From these two tables, it can be observed that

	Initial Guess	Spring Configuration		
		I	II	III
l_{01} (m)	0.1	0.130	0.316	
l_{02} (m)	0.1	0.182		0.186
l_{03} (m)	0.1		0.216	
l_{04} (m)	0.1			0.500
k_1 (kN/m)	0	29.5	10.2	
k_2 (kN/m)	0	50.0		50.0
k_3 (kN/m)	0		42.6	
k_4 (kN/m)	0			48.8

TABLE 2: Design variables of the springs

	Initial Guess	Spring Configuration		
		I	II	III
s_1(m)	0	0.150	-0.100	
s_{21}(m)	0.1	0.017		0.038
s_{22}(m)	0.1	0.233		0.233
s_3(m)	0.35		0.548	
s_4(m)	0.30			0.576

TABLE 3: Location Variables of the springs

springs k_1 for the first configuration is shorter than for the second configuration, because spring k_1 in the first configuration must provide a larger side force to cancel that generated by spring k_2. Springs k_2 used in the first and third configurations are attached at almost the same positions, i.e., G' and G coincide. The location of D' for spring k_3, which is 0.548 meters below joint B_0, does not come too close to the ground because the leg is about 0.8 meter long. Since s_4 is about 0.576 meter (much larger than the width of the leg), there may not be enough room to attach springs k_4 for the third configuration. Table 4 shows the maximal crank torques and actuating forces for the three alternative designs with and without springs. As shown in Table 4, the actuating torque and force values for the second configuration have been reduced to about half of the values without springs.

	Without Springs	Spring Configurations		
		I	II	III
f_{86Y}(kN)	2.75	2.22	1.38	1.69
T (N-m)	7.93	6.44	4.01	4.92

TABLE 4: Actuating force and torque with and without springs

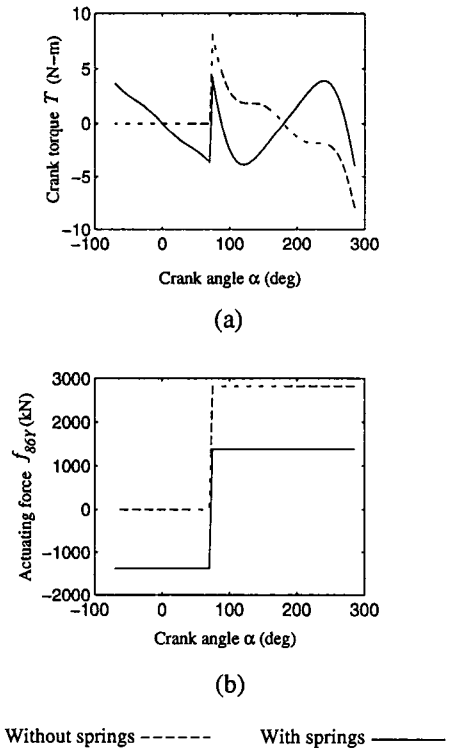

FIGURE 5: A comparison of actuating forces and torques: (a) Crank torque vs. crank angle; (b) Actuating force vs. crank angle

From the above discussions, we conclude that the second spring configuration is the most promising design. For this configuration, Figs. 5(a) and 5(b) show the reduction in crank torque and actuating force, respectively, for a full walking cycle. Although the torque and force in the returning portion are increased, they are reduced significantly in the propelling portion of the walking path.

5 SUMMARY

We present the results of a two-stage optimization study for a planar two-DOF leg mechanism. In the first stage, leg mechanism dimensions are determined via a multiobjective optimization procedure to achieve three design goals: minimum leg size, minimum actuating force, and minimum peak crank torque. The dimensional synthesis of such a complicated leg mechanism is accomplished without the need for a prescribed coupler-point path. In the second stage, the actuating force and torque are further reduced by the attachment of tension springs. Three different configurations for the placement of springs are considered. The spring attachment points and spring sizes are optimized via an optimization model for the entire walking cycle. It is concluded that the actuating force and torque can be sustantially reduced with the inclusion of tension springs.

6 ACKNOWLEDGMENT

The work presented here was supported in part by the National Science Foundation, Grant No. EID-9212126.

REFERENCES

Alexander, R. M., 1990, "Three Uses for Springs in Legged Locomotion," The International Journal of Robotics Research, Vol. 9, No. 2, pp. 53–61.

Dhandapani, S., and Ogot, M., 1994, "Modeling of a Leg System to Illustrate the Feasibility of Energy Recovery in Walking Machines," *Advances in Design Automation*, DE-Vol. 69-2, ASME Pub., pp. 429–436.

Fan, M. K. H., Wang, L. S., Koninckx, J., and Tits, A. L., 1990, *CONSOLE - User's Manual*, Version 1.1, SRC-TR-87-212r2, Institute for Systems Research, University of Maryland, College Park, Maryland.

Funabashi, H., Ogawa, K., Gotoh, Y., and Kojima, K., 1985a, "Synthesis of Leg-Mechanisms of Biped Walking Machines (Part I, Synthesis of Ankle-Path-Generator)," Bulletin of JSME, Vol. 28, No. 237, pp. 537–543.

Funabashi, H., Ogawa, K., Gotoh, Y., and Kojima, K., 1985b, "Synthesis of Leg-Mechanisms of Biped Walking Machines (Part II, Synthesis of Foot-Driving Mechanism)," Bulletin of JSME, Vol. 28, No. 237, pp. 544–549.

Hartenberg, R., and Denavit, J., 1964, *Kinematics Synthesis of Linkages*, McGraw-Hill, New York, New York.

Hirose, S., 1984, "A study of Design and Control of a Quadruped Walking Vehicle," The International Journal of Robotics Research, Vol. 3, No. 2, pp. 113–133.

Matthew, G., and Tesar, D., 1977a, "Synthesis of Spring Parameters to Satisy Specified Energy Levels in Plannar Mechanisms," ASME Journal of Engineering for Industry, pp. 341–346.

Matthew, G., and Tesar, D., 1977b, "Synthesis of Spring Parameters to Balance General Forcing Functions in Plannar Mechanisms," ASME Journal of Engineering for Industry, pp. 347–352.

Pugh, D., Ribble, E., Vohnout, V., Bihari, T., Walliser, T., Patterson, M., and Waldron, K., 1990, "Technical Description of the Adaptive Suspension Vehicle," The International Journal of Robotics Research, Vol. 9, No. 2, pp. 24–51.

Shieh, W., Azarm, S., Tsai, L., and Tits, A., 1994, "Optimization-Based Design of a Leg Mechanism via Combined Mechanism and Structural Analysis," *Advances in Design Automation*, DE-Vol. 69-1, ASME Pub., pp. 199–209.

Shin, E., and Streit, D., 1993, "An Energy Efficient Quadruped with Two-Stage Equilibrator," ASME Journal of Mechanical Design, Vol. 115, No. 1, pp. 156–163.

Todd, D., 1985, *Walking Machines - An Introduction to Legged Robots*, Chapman and Hall.

Waldron, K., Vohnout, V., Pery, A., and McGhee, R., 1984, "Configuration Design of the Adaptive Suspension Vehicle," The International Journal of Robotics Research, Vol. 3, No. 2, pp. 37–48.

Williams, R. P., Tsai, L. W., and Azarm, S., 1991, "Design of a Crank-and-Rocker Driven Pantograph: A Leg Mechanism for the University of Maryland's 1991 Walking Robot," *Proc. of 2nd Nat. Conf. on Applied Mechanisms and Robotics*, Vol. 1, Paper No. VIB.2, Cincinnati, Ohio.

NOMENCLATURE

$\mathtt{C}i$:= ith constraint.
$\mathbf{e}_i$:= unit vector with the orientation angle θ_i, i.e., $\mathbf{e}_i = [\cos(\theta_i) \quad \sin(\theta_i)]$.
$\mathbf{e}_X$:= unit vector of X-axis.
$\mathbf{e}_Y$:= unit vector of Y-axis.
f_{ijX} := X-component of $\mathbf{f}_{ij}$.
f_{ijY} := Y-component of $\mathbf{f}_{ij}$.
$\mathbf{f}_{ij}$:= force (vector) applied by links i on j.
$\mathtt{FC}i$:= ith functional constraint.
$\mathtt{FO}i$:= ith functional objective.
$\mathtt{H}_{\mathtt{C}i}$:= threshold value for the ith hard constraint.
$\mathtt{H}_{\mathtt{FC}i}$:= threshold value for the ith hard functional constraint.
l_i := stretched length of the ith spring.
l_{0i} := unstretched length of the ith spring.
k_i := spring constant of the ith spring.
n := amplification factor ($=x_5/x_4$).
$\mathtt{O}i$:= ith objective.
R_p := crank angle range of the propelling portion of the foot-point path.
s_1 := $\overline{FF'}$
s_{21} := $\overline{FG'}$
s_{22} := $\overline{BC'}$
s_3 := $\overline{B_0D'}$
s_4 := $\overline{C''C'''}$
s_h := horizontal stride length, 0.30 m (12 in).
s_v := vertical stride length, 0.20 m (8 in).
T := crank torque, N-m.
x_i := design variable, i=1, ..., 5 (see Fig. 1).
$\mathbf{x}$:= vector of all the design variables.
$X_{(\cdot)}$:= X coordinate of point $(\cdot)$.
$Y_{(\cdot)}$:= Y coordinate of point $(\cdot)$.
α := crank angle (see Fig. 1).
θ_i := orientation angle of link indicated in Fig. 1, i= 0, 1, ... , 7.

APPENDIX A

Derivation of the Coordinates of Points C and E

The X- and Y-coordinates of the coupler point C in the reference frame, as shown in Fig. 1, can be written as

$$X_C = \overline{B_0B}\cos(\theta_2) + \overline{BC}\cos(\pi/2 - \phi/2 + \theta_3) \tag{A.1}$$

$$Y_C = \overline{B_0B}\sin(\theta_2) + \overline{BC}\sin(\pi/2 - \phi/2 + \theta_3) \tag{A.2}$$

where $(\pi/2 - \phi/2 + \theta_3)$ is the orientation angle of the vector $\overrightarrow{BC}$ and

$$\theta_2 = \frac{\phi}{2} - \angle AB_0A_0 + \frac{1}{2}\angle ABB_0 \tag{A.3}$$

$$\theta_3 = \frac{\pi}{2} - \angle AB_0A_0 - \frac{1}{2}\angle ABB_0. \tag{A.4}$$

Substituting Eqs. (A.3)-(A.4) and $\overline{B_0B} = \overline{BC} = x_3$ into Eqs. (A.1)-(A.2) yields

$$X_C = 2x_3\sin(\angle AB_0A_0)\sin(\frac{1}{2}\angle ABB_0 + \frac{1}{2}\phi) \tag{A.5}$$

$$Y_C = 2x_3\cos(\angle AB_0A_0)\sin(\frac{1}{2}\angle ABB_0 + \frac{1}{2}\phi). \tag{A.6}$$

The quantities $\angle AB_0A_0$ and $\angle ABB_0$ are obtained via the sine law for ΔAB_0A_0 and ΔABB_0, respectively:

$$\angle AB_0A_0 = \sin^{-1}\{\frac{\sin(\alpha)}{[(x_2/x_1)^2 - 2(x_2/x_1)\cos(\alpha)+1]^{1/2}}\} \tag{A.7}$$

$$\frac{1}{2}\angle ABB_0 = \sin^{-1}\{\frac{[(x_2/x_1)^2 - 2(x_2/x_1)\cos(\alpha)+1]^{1/2}}{2(x_3/x_1)}\} \tag{A.8}$$

Then, the coordinate of the coupler point C (X_C, Y_C), is obtained by substituting Eqs. (A.7) and (A.8) into (A.5) and (A.6), as

$$X_C = x_1\sin(\alpha)\{\cos(\phi/2) + V\sin(\phi/2)\} \tag{A.9}$$

$$Y_C = [x_2 - x_1\cos(\alpha)]\{\cos(\phi/2) + V\sin(\phi/2)\} \tag{A.10}$$

where

$$V = [\frac{(2x_3/x_1)^2}{(x_2/x_1)^2 - 2(x_2/x_1)\cos(\alpha) + 1} - 1]^{1/2}. \tag{A.11}$$

From the two triangles, ΔCFD and ΔDHE as shown in Fig. 1, the coordinates of E and C are related by $X_E = -nX_C$ and $Y_E = Y_D + n(Y_D - Y_C)$. Thus, the foot-point coordinates are

$$X_E = -nx_1\sin(\alpha)\{\cos(\phi/2) + V\sin(\phi/2)\} \tag{A.12}$$

$$Y_E = (1+n)Y_D - n[x_2 - x_1\cos(\alpha)]\{\cos(\phi/2) + V\sin(\phi/2)\}. \tag{A.13}$$

APPENDIX B

Derivation of Crank Torque T and Force $\mathbf{f}_{86}$ for the First Spring Configuration

From the principle of virtual work and stationary energy,

$$\delta W = \delta P \tag{B.1}$$

where δW is the virtual work and δP is the virtual potential energy. The potential energy stored by the springs is

$$P = 1/2\, k_1(l_1 - l_{01})^2 + 1/2\, k_2(l_2 - l_{02})^2. \tag{B.2}$$

Differentiating Eq. (B.2) results in

$$\delta P = k_1(l_1 - l_{01})\delta l_1 + k_2(l_2 - l_{02})\delta l_2. \tag{B.3}$$

The square of l_1 can be written from Fig. 4(a), as

$$l_1{}^2 = [X_C^2 + (Y_C - s_1)^2] \tag{B.4}$$

while the square of l_2 can be obtained by applying the cosine law to $\Delta F'FG$ and ΔCDF as

$$l_2{}^2 = s_{21}{}^2 + s_{22}{}^2 - \frac{s_{21}s_{22}}{x_4{}^2}[(Y_D - Y_C)^2 + X_C{}^2 - 2x_4{}^2]. \tag{B.5}$$

From Eqs. (B.4) and (B.5) $\min(l_1)$, $\min(l_2)$, $\max(l_1)$, and $\max(l_2)$ could be obtained. Differentiating Eqs. (B.4) and (B.5) and substituting the resulting equations in Eq. (B.3), yields

$$\delta P = k_1\delta_1[X_C\frac{dX_C}{d\alpha} + (Y_C - s_1)\frac{dY_C}{d\alpha}]\delta\alpha - k_2\delta_2(Y_D - Y_C)\delta Y_D + k_2\delta_2[-X_C\frac{dX_C}{d\alpha} + (Y_D - Y_C)\frac{dY_C}{d\alpha}]\delta\alpha\delta Y_D \tag{B.6}$$

where $\delta_1 = 1 - l_{01}/l_1$ and $\delta_2 = (s_{21}s_{22}/x_4{}^2)(1 - l_{02}/l_2)$. Now, consider the virtual work of the leg mechanism,

$$\delta W = T\delta\alpha + \mathbf{f}_{05} \cdot \delta\mathbf{r}_{B_0E} + \mathbf{f}_{86} \cdot \delta\mathbf{r}_{B_0D}. \tag{B.7}$$

Since $\mathbf{f}_{05} = f_{05X}\mathbf{e}_X + f_{05Y}\mathbf{e}_Y$, $\mathbf{f}_{86} = f_{86X}\mathbf{e}_X + f_{86Y}\mathbf{e}_Y$, $\mathbf{r}_{B_0E} = -nX_C\mathbf{e}_X + [(1+n)Y_D - nY_C]\mathbf{e}_Y$, and $\mathbf{r}_{B_0D} = Y_D\mathbf{e}_Y$, the virtual work is given:

$$\begin{aligned}\delta W =& (T - nf_{05X}\frac{dX_C}{d\alpha} - nf_{05Y}\frac{dY_C}{d\alpha})\delta\alpha + \\ & [(1+n)f_{05Y} + f_{86Y}]\delta Y_D.\end{aligned} \tag{B.8}$$

Substituting Eqs. (B.8) and (B.6) into (B.1) and set the coefficients of $\delta\alpha$ and δY_D to zero, yields

$$T = [nf_{05X} + (k_1\delta_1 - k_2\delta_2)X_C]\frac{dX_C}{d\alpha} + [nf_{05Y} + k_1\delta_1(Y_C - s_1) + k_2\delta_2(Y_D - Y_C)]\frac{dY_C}{d\alpha} \tag{B.9}$$

and

$$f_{86Y} = -(1+n)f_{05Y} - k_2\delta_2(Y_D - Y_C). \tag{B.10}$$

The side force f_{86X} can be found by taking the moment about point C of the forces acting on the pantograph,

$$f_{86X} = -(1+n)f_{05X} + k_2\delta_2X_C. \tag{B.11}$$

Finally, summing all the forces acting on pantograph, yields

$$\begin{aligned} f_{34X} &= nf_{05X} - k_2\delta_2X_C \\ f_{34Y} &= nf_{05Y} + k_2\delta_2(Y_D - Y_C). \end{aligned} \tag{B.12}$$